JJAP

Independent Control of the Thermoelectric Parameters in Titanium Nitride Thin Films via Crystal Preferred Orientation Control Using the Combinatorial Sputter Coating

Michiko Sasaki[1*], Yibin Xu[2], Takao Mori[1] and Masahiro Goto[1*]

[1] *Thermal Energy Materials Group, Research Center for Materials Nanoarchitectonics (MANA), National Institute for Materials Science, 1-2-1 Sengen, Tsukuba, Ibaraki 305-0047, Japan.*
[2] *Data-driven Inorganic Materials Group, Center for Basic Research on Materials, National Institute for Materials Science (NIMS) , 1-2-1 Sengen, Tsukuba, Ibaraki 305-0047, Japan.*

[*]*Email: sasaki.michiko@nims.go.jp, goto.masahiro@nims.go.jp*

To clarify the effect of deposition conditions on crystallographic orientation and thermoelectric properties at room temperature (300 K), titanium nitride (TiN) thin films were systematically fabricated via combinatorial reactive sputtering while varying the Ar/N_2 gas mixing ratio over a wide range of 0%–100%. Although the overall film composition remained nearly constant except for the N-free condition, significant changes in crystallographic orientation, grain growth behavior, and transport properties were observed as a function of nitrogen partial pressure. X-ray diffraction (XRD) analysis revealed two characteristic trends in orientation evolution with inflection points at N fractions of approximately 70% and 40%. The Seebeck coefficient increased monotonically with decreasing nitrogen fraction and exhibited a weak correlation with the crystallographic orientation. In contrast, electrical resistivity exhibited a strong correlation with orientation-dependent XRD peak intensity changes, resulting in the partial decoupling of the conventional trade-off between the Seebeck coefficient and resistivity. Consequently, the power factor was optimized without significant compositional modification. Thermal conductivity also exhibited obvious dependence on crystallographic orientation and grain structure, contributing to thermoelectric performance optimization. Consequently, a maximum dimensionless figure of merit of 0.025 was achieved. These results demonstrate that crystallographic orientation and microstructural control via deposition process optimization is an effective strategy for mitigating the correlations between thermoelectric parameters in TiN thin films. This approach provides useful design guidelines for nitride-based thin-film thermoelectric materials operating at room temperature.

1. Introduction

In recent years, there has been an increasing focus on technologies that recover unused waste heat dissipated from industrial equipment, electronic devices, and mobile vehicles[1-5]. This focus is underpinned by the recognition of the importance of improving energy utilization efficiency and decarbonization. The thermoelectric conversion process is based on the Seebeck effect, which generates an electromotive force due to temperature differences. This enables a direct conversion between heat and electricity without the need for moving mechanical parts. Consequently, this method is expected to be a compact and highly reliable energy harvesting technique. The performance of thermoelectric materials is generally evaluated using the dimensionless performance index ($zT = S^2/\rho\kappa$, T). Achieving an optimal balance between the Seebeck coefficient (S), electrical resistivity (ER) (ρ), and thermal conductivity (κ) is imperative. Consequently, optimizing one parameter to enhance zT often leads to compensatory changes in another, leading to a trade-off.However, these properties involve inherent trade-offs, making it difficult to achieve high performance.

To mitigate these trade-offs, research has advanced toward reducing lattice thermal conductivity via interfacial scattering through dimensionality reduction, thin-film fabrication, and nanostructuring while optimizing electrical transport properties via quantum confinement and band structure control[6-9]. The

deposition process of thin-film thermoelectric materials is of particular significance, because it allows precise control of microstructural features, such as crystallographic orientation, defect density, stress levels, and grain boundary density. Consequently, these materials are the focal point of material exploration and process optimization for energy harvesting applications operating at ambient temperatures (300 K), including environmental waste heat, heat sources in proximity to the human body, and device self-heating.

Recently, transition metal nitrides (TMNs) have attracted attention as potential candidate thin-film thermoelectric materials. TMNs typically exhibit a combination of material stability, characterized by elevated melting points, corrosion resistance, and mechanical strength, along with electrical properties that are amenable to control via film deposition. The potential of these materials as a class of energy harvesting materials, including thermoelectric and piezoelectric applications, is a subject of current discussion. High power factors have been achieved for ScN-[10, 11] and CrN-based[12-14] thin films. In addition, material design guidelines based on nitride thin films are currently being established.

This study focuses on titanium nitride (TiN), which serves as a representative example of TMNs. The material under investigation exhibits a rock salt structure, metallic conductivity, and high thermal stability. In recent years, there has been a growing body of research focusing on the room-temperature thermoelectric properties of TiN thin films fabricated via atomic layer deposition[15, 16]. Ssennyimba et al. reported that TiN can control thermal and electrical transport through light[17]. In addition, Okubo et al. combined Bayesian optimization (machine learning) with MO-MBE to efficiently explore growth conditions for TiN epitaxial thin films and optimize the process[18].

These studies have demonstrated the potential for achieving significant power factors at room temperature under specific deposition conditions. Consequently, TiN has emerged as a promising candidate material, warranting re-evaluation as a room-temperature thermoelectric conversion material, in addition to its prevailing applications as a "highly conductive and highly stable" material. However, current zT values remain far below the levels required for practical applications, necessitating a breakthrough.

Conversely, for TiN thin films deposited by physical vapor deposition, typically sputtering, deposition conditions, such as the partial pressure of reactive gas (N_2) and the Ar/N_2 ratio, result in variations in the composition (TiN_x), crystalline phase, crystallographic orientation, defects (vacancies, excess nitrogen), and impurity incorporation (Ar). Consequently, transport properties, including electrical resistivity, fluctuate significantly. To illustrate this point, consider the example of reactive sputtering, where the nitrogen flow rate and orientation (111, 200, etc.) significantly affect resistivity. Moreover, as the nitrogen amount increases, the phase changes from α-Ti to ε-Ti_2N to δ-TiN, and the electrical resistivity changes accordingly, corresponding to phase formation. In addition, the Ar/N_2 flow ratio can influence the orientation and resistivity. Alterations in the Ar/N_2 ratio result in fluctuations in the preferred orientation balance between the 111 and 200 directions, thereby inducing resistivity changes. Furthermore, film deposition under mixed Ar/N_2 discharge conditions may involve Ar incorporation and excess nitrogen contamination. This may affect thermoelectric transport via carrier scattering and defect chemistry.

Consequently, when developing TiN thin films for use as thermoelectric conversion materials, comprehensively comprehending the impact of deposition conditions, particularly the Ar/N_2 mixture ratio in reactive sputtering, on the composition, phase, orientation, and defects is imperative. This affects S, ρ, and ultimately the power factor at room temperature (300 K). However, studies that have systematically scanned the Ar/N_2 mixture ratio over a wide range (0%–100%) and consistently organized the correlation between thermoelectric properties at room temperature and microstructure/electrical properties are limited. Therefore, optimizing the experimental design to explore the optimal process window is critical because this approach may help mitigate the trade-offs between thermoelectric parameters within a given crystalline structure domain.

To address this challenge, combinatorial deposition and high-throughput evaluation have been established as powerful methodologies for rapidly exploring multidimensional process space and extracting composition–process–structure–property correlations. Material discovery and optimization can be accelerated by fabricating a thin-film material library in batches, accompanied by property mapping across continuous condition gradients.

In this study, TiN thin films were fabricated via combinatorial sputtering. A constant radio frequency (RF) power must be maintained while systematically varying the mixing ratio of the sputtering gas mixture (Ar and N_2) over a range of 0%–100%. The thermoelectric properties (Seebeck coefficient, electrical properties, and power factor when necessary) of the obtained thin films were evaluated at 300 K. The objective of this study is to clarify the correlation between transport property variations caused by the mixing ratio and the composition, crystal phase, orientation, and defect state. The establishment of design guidelines and optimal deposition conditions for TiN thin films as room-temperature thermoelectric materials will help expand the material base for nitride

thin-film thermoelectrics.

2. Experiment

The sample substrates used in this study were synthetic quartz and a magnesium oxide single crystal (100) (4 × 22 × 1.5 mm) with a mirror-polished surface. These sample substrates were secured within the sample holder of the combinatorial sputter coating system (COSCOS)[19-38] shown in **Fig. 1**. The coating parameters are presented in **Table I**. The system was evacuated until the ultimate pressure reached 5.0 x 10^{-5} Pa or lower. Film deposition was performed via magnetron sputtering under the following conditions: a process gas pressure of 0.4 Pa, RF power of 100 W, and target–substrate distance of 55 mm. The process gas mixture was composed of Ar/N_2, with the Ar/N_2 ratio varying from 0% to 100%. The target used for the deposition process was a 50-mm-diameter TiN (Fruuchi Chemical Co.,99%) sample. The thickness of the deposited film was approximately 400 nm.

Thermoelectric properties such as the Seebeck coefficient, resistivity, and thermal conductivity were measured using a thermoelectric property measurement system (Advance Riko Co., type-ZEM-3) and ω-type thermal conductivity measurement equipment[30, 39, 40]. The crystal structure of the samples was measured by X-ray diffraction (XRD, Rigaku; SmartLab) with Cu Ka (1.54 Å) radiation at an incident angle of 0.5°. The chemical composition of the samples was measured via X-ray photoelectron microscopy (ESCA3400, Shimadzu Corporation).

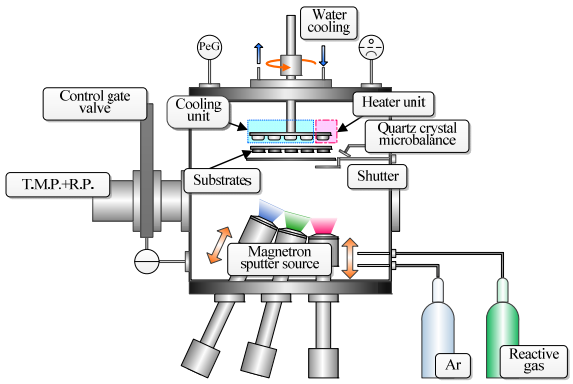


Fig.1. Schematic illustration of combinatorial sputter coating system (COSCOS).

3. Results and Discussion

In this study, TiN thin films with systematically varied physical characteristics were successfully fabricated using a COSCOS. **Figure 2** shows images of TiN thin films deposited while varying the mixing ratio of nitrogen and argon gases in the process gas. As the fraction of N_2 gas decreased, the color of the TiN films changed from black to gold. Because the film thickness was fixed at 400 nm for all samples, this color change

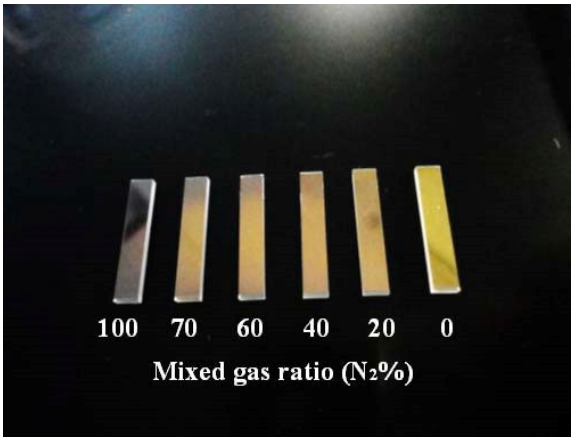


Fig.2. Photographs of TiN thin films systhesized while varying the mixing ratio of nitrogen and argon gases in the sputter gas.

cannot be attributed to optical interference effects; however, this change originates from crystallographic orientation differences.

For the sample deposited at 100% nitrogen partial pressure, the resulting film was unstable and delaminated over time. Consequently, part of the

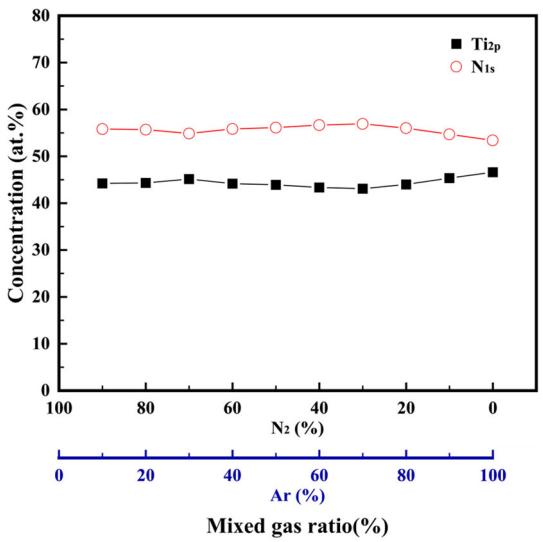


Fig. 3 Compositional variation of TiN thin films as a function of the process gas mixing ratio.

physical property characterization could not be performed for this sample. **Figure 3** shows the compositional variation of TiN thin films as a function of the process gas mixing ratio. Overall, no drastic compositional changes were observed. For the sample deposited with 0% N_2, the Ti/N ratio was 0.87, which is comparable to the stoichiometric composition of TiN. When the N_2 fraction exceeded 20%, the Ti and N contents in the films remained nearly constant, and the nitrogen content was approximately 11%–14% higher than the titanium content. The ESCA compositional

analysis performed this time evaluated a depth of 3 nm from the surface. Since it is unavoidable to avoid the effect of oxydation from the surface due to atmospheric exposure, approximately 14% of oxygen remained in all samples. However, the oxygen content decreased continuously and rapidly from 28% at the surface to approximately half that amount. Furthermore, since the film was deposited at a background pressure of 5.0 x 10^{-5} Pa, oxidation within the film during deposition is negligible. Consequently, the oxidation layer is confined to the very surface layer, and it is unlikely to significantly affect the thermoelectric properties.

Figure 4 presents the XRD spectra of TiN samples deposited at different nitrogen partial pressures. Diffraction peaks corresponding to the 111, 200, 220, 311, 222, and 400 planes of TiN were observed. The

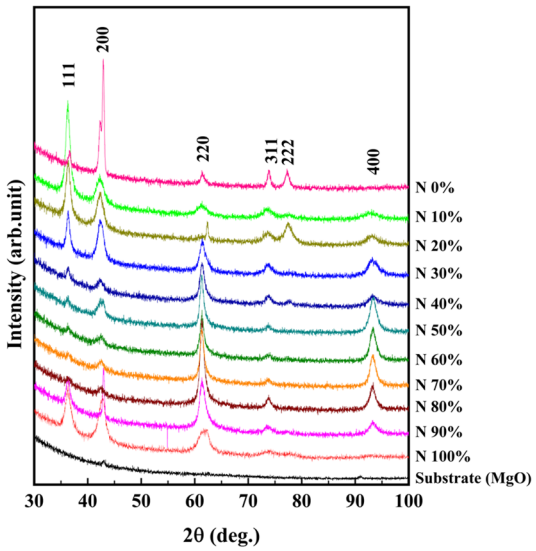


Fig. 4 X-ray diffraction (XRD) spectra of TiN samples deposited under different nitrogen partial pressures.

intensities of these peaks changed systematically with nitrogen partial pressure. At 100% nitrogen partial pressure, the 111 and 200 peak intensities were high. These intensities decreased as the nitrogen partial pressure was reduced to 70%, reached a minimum, and then increased again as the pressure approached 0%. In contrast, the 220 and 400 peak intensities increased as the pressure decreased from 100% to 70%, reached a maximum, and subsequently decreased. Another distinct trend was observed for the 222 peak, which appeared at 40% nitrogen and exhibited an increasing intensity and a decreasing full width at half maximum as the nitrogen fraction approached 0%. This behavior suggests significant grain growth for crystallites contributing to the 222 orientation. These results indicate that the changes in XRD peak intensities with nitrogen partial pressure are governed by the superposition of two distinct trends.

Figure 5 shows the dependence of the Seebeck coefficient, resistivity, and power factor on the mixed gas ratio[41]. The Seebeck coefficient increased linearly with decreasing nitrogen partial pressure. In contrast, the electrical resistivity decreased rapidly as the nitrogen fraction decreased from 90% to 70%, increased again at approximately 40%, and then decreased toward 0%. The power factor reached a maximum at 70% nitrogen partial pressure, decreased toward 40%, and then increased again.

A particularly notable finding is the correlation with crystallographic orientation evaluated by XRD. Although the Seebeck coefficient exhibited no correlation with the changes in the XRD peak intensities and only a monotonic increase, the electrical resistivity exhibited a strong correlation. As described above, inflection points in the XRD peak intensity evolution were observed at nitrogen fractions of approximately 70% and 40%, and the resistivity

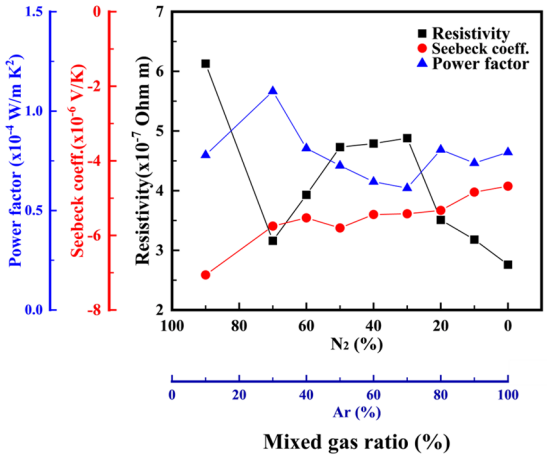


Fig. 5 Dependence of the Seebeck coefficient, resistivity, and power factor on the mixed gas ratio.

exhibited inflection points at nearly the same compositions. This finding indicates that the normally positive correlation between the Seebeck coefficient and electrical resistivity was effectively decoupled in this system. These results demonstrate that the power factor can be optimized via crystallographic orientation control even without significant changes in composition or elemental species. Changes in nitrogen partial pressure are thought to cause alterations in the nitrogen content within the film, specifically in nitrogen deficiency levels and associated point defect concentrations. Generally, it is known that a decrease in carrier concentration leads to an increase in the Seebeck coefficient. The monotonically increasing behavior observed in this study may reflect a continuous change in carrier concentration due to subtle variations in nitrogen content, rather than a crystal orientation effect. Therefore, the existence of different governing factors is suggested: the Seebeck coefficient depends primarily on stoichiometric composition and defect concentration, while electrical resistivity is additionally strongly influenced by crystal orientation. This is considered the

reason why the correlation between the Seebeck coefficient and electrical resistivity is effectively decoupled in this system.

Figure 6 shows the thermal conductivity of the TiN samples as a function of nitrogen partial pressure, revealing a strong correlation with the changes in the crystallographic orientation observed by XRD. As the nitrogen fraction decreased from 90% to 70%, the thermal conductivity decreased and then increased toward 50%. This trend correlates with one of the two previously discussed XRD peak intensity variation trends. In contrast, the thermal conductivity measurements of the 40% nitrogen sample were unstable and exhibited significant errors. This behavior was reproducible across different measurement locations and repeated trials, confirming its origin in the sample. Notably, this composition corresponds to the second inflection point observed in the XRD peak intensity evolution. Beyond this 40% threshold, thermal conductivity decreased again. The 40% sample did not exhibit any particular peculiarities compared to other samples, especially regarding surface roughness, heterogeneity, or substrate adhesion. However, nearly all XRD peak intensities were lower, indicating a sample with a microcrystalline-amorphous structure. As a result, the zT value for the 40% sample in question contains an error of approximately 40%. These results suggest that changes in interfacial conditions and interface density, as well as variations in carrier mobility associated with changes in crystallographic orientation and grain size, significantly affect phonon scattering and heat-carrying electrons[33, 42-52]. Therefore, thermal conductivity can also be optimized via crystallographic orientation control.

Figure 7 shows the dependence of the thermoelectric figure of merit (zT) on the Ar gas partial pressure. A maximum zT value of 0.025 was obtained at an Ar fraction of 30%, which is consistent with the observed trend for the power factor. In addition, at an Ar fraction of 80%, the zT value increased to 0.021, primarily due to a reduction in thermal conductivity. Although the absolute zT value is insufficient for direct application in thermoelectric devices, the significance of this study lies in demonstrating that, in a simple material system such as TiN with minimal compositional variation, the correlations between thermoelectric parameters can be relaxed by controlling the crystallographic orientation and grain structure.

4.Conclusion

TiN thin films were systematically fabricated by combinatorial sputtering while varying the Ar/N_2 gas mixing ratio over a wide range. The effects of the deposition conditions on the crystallographic orientation and thermoelectric properties at room temperature were investigated. Although the overall film composition remained nearly constant except for the N_2-free condition, marked changes in

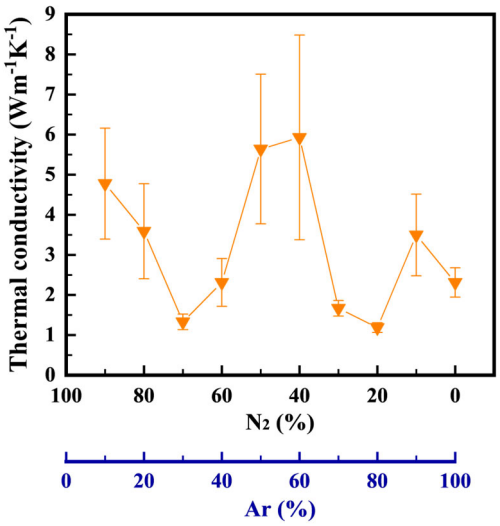


Fig. 6 Nitrogen partial pressure dependence of the thermal conductivity of TiN samples.

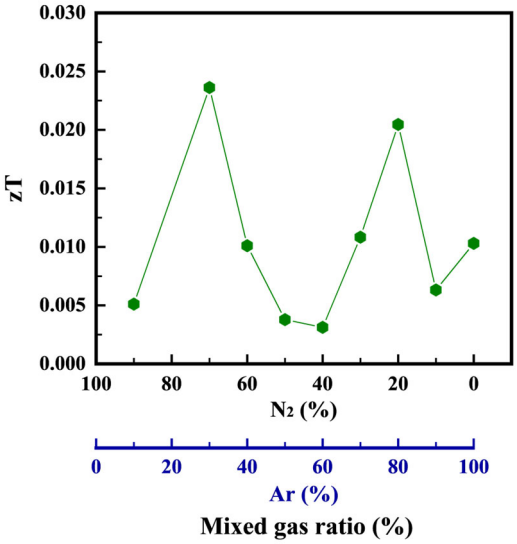


Fig. 7 Dependence of the thermoelectric figure of merit, zT, on the Nitrogen gas partial pressure.

crystallographic orientation, grain growth behavior, and transport properties were observed as a function of nitrogen partial pressure. XRD analysis revealed two characteristic orientation evolution trends with inflection points around N_2 fractions of approximately 70% and 40%, indicating complex microstructural transitions induced by the gas mixture ratio.

The Seebeck coefficient increased monotonically with decreasing nitrogen fraction and exhibited a weak correlation with the crystallographic orientation. In contrast, electrical resistivity exhibited a strong correlation with the orientation-dependent XRD peak intensity changes, resulting in the partial decoupling of the conventional trade-off between the Seebeck coefficient and resistivity. The power factor was successfully optimized without significant

compositional modification. Thermal conductivity also exhibited obvious dependence on crystallographic orientation and grain structure, further contributing to thermoelectric performance optimization. Consequently, a maximum zT value of 0.025 was achieved. Although the magnitude of the zT value is insufficient for direct application in thermoelectric devices, it demonstrates that, in simple material systems such as TiN with minimal compositional variation, the correlation between thermoelectric parameters can be mitigated by controlling the crystallographic orientation and grain structure. This finding can lead to improvements in the performance of complex thermoelectric materials with zT values approaching practical levels.

These results demonstrate that crystallographic orientation and microstructural control via deposition process optimization is an effective strategy for relaxing the correlations between thermoelectric parameters in TiN thin films. This approach is also applicable to enhancing the zT value of high-performance nitride thermoelectric materials such as ScN and CrN, providing useful design guidelines for nitride-based thin-film thermoelectric materials operating at room temperature.

Acknowledgements

This research was supported by Japan Science and Technology Agency (JST) under the Future Society Creation Project, Grant Number JPMJMI19A1, CREST under the projects “Exploring Innovative Materials in Unknown Search Space” (JPMJCR21O2), and Grant-in-Aid for Scientific Research (C) 24K07349 and 25K08337 from the Japan Society for the Promotion of Science (JSPS).

References

1) P. Fernández-Yáñez, V. Romero, O. Armas and G. Cerretti: Appl Therm Eng. **196** (2021) [in English].
2) T. Hendricks, T. Caillat and T. Mori: Energies. **15** [19](2022) [in English].
3) C.T. Kuah, Q.Y. Koh, S. Rajoo and K.Y. Wong: Environ Sci Pollut R. **30** [28](2023)72074. [in English].
4) Y.T. Hao, H.J. Zhou, T. Tian, W. Zhang, X. Zhou, Q.F. Shen, T. Wu and J. Li: Appl Energ. **384** (2025) [in English].
5) H.R. Rahbari, B. Elmegaard, E. Bellos, C. Tzivanidis and A. Arabkoohsar: Renew Sust Energ Rev. **215** (2025) [in English].
6) L.D. Hicks and M.S. Dresselhaus: Phys Rev B Condens Matter. **47** [24](1993)16631.
7) L.D. Hicks and M.S. Dresselhaus: Phys Rev B Condens Matter. **47** [19](1993)12727.
8) L.D. Hicks, T.C. Harman, X. Sun and M.S. Dresselhaus: Phys Rev B Condens Matter. **53** [16](1996)R10493.
9) R. Jha, N. Tsujii, A. Riss, M. Parzer, E. Bauer, T. Baba and T. Mori: Sci Technol Adv Mat. **26** [1](2025) [in English].
10) S. Kerdsongpanya, N.V. Nong, N. Pryds, A. Zukauskaite, J. Jensen, J. Birch, J. Lu, L. Hultman, G. Wingqvist and P. Eklund: Appl Phys Lett. **99** [23](2011) [in English].
11) D. Rao, B. Biswas, E. Flores, A. Chatterjee, M. Garbrecht, Y.R. Koh, V. Bhatia, A.I.K. Pillai, P.E. Hopkins, M. Martin-Gonzalez and B. Saha: Appl Phys Lett. **116** [15](2020) [in English].
12) M.A. Gharavi, D. Gambino, A. le Febvrier, F. Eriksson, R. Armiento, B. Alling and P. Eklund: Mater Today Commun. **28** (2021) [in English].
13) N.A.M. Sabeer and P.P. Pradyumnan: Mater Sci Eng B-Adv. **273** (2021) [in English].
14) T. Aizawa, F.F. Yun and T. Mori: Acs Appl Energ Mater. **8** [18](2025)13360. [in English].
15) P. Goel, C. Kauppinen, R. Raju and I. Tittonen: Nanoscale Adv. (2025) [in English].
16) W. Tsai, M. Delfino, J.A. Fair and D. Hodul: J Appl Phys. **73** [9](1993)4462. [in English].
17) K.W. Ssennyimba, S.S. Liao, Y.X. Zhu, T.J. Legvold, D.T. Lowder, K. Pagadala, A. Boltasseva, V.M. Shalaev and D. Natelson: Apl Mater. **13** [8](2025) [in English].
18) I. Ohkubo, Z. Hou, J.N. Lee, T. Aizawa, M. Lippmaa, T. Chikyow, K. Tsuda and T. Mori: Mater Today Phys. **16** (2021) [in English].
19) M. Goto, A. Kasahara and M. Tosa: Vacuum. **80** [7](2006)740. [in English].
20) M. Goto, A. Kasahara and M. Tosa: Appl Surf Sci. **252** [7](2006)2482. [in English].
21) M. Goto, A. Kasahara and M. Tosa: Jpn J Appl Phys. **47** [12](2008)8914. [in English].
22) Y.B. Xu, R. Kato and M. Goto: J Appl Phys. **108** [10](2010) [in English].
23) M. Goto, A. Kasahara and M. Tosa: Tribol Lett. **43** [2](2011)155. [in English].
24) Y.B. Xu, M. Goto, R. Kato, Y. Tanaka and Y. Kagawa: J Appl Phys. **111** [8](2012) [in English].
25) M. Goto, M. Sasaki, A. Kasahara and M. Tosa: Tribol Lett. **55** [2](2014)289. [in English].
26) T.Z. Zhan, Y.B. Xu, M. Goto, Y. Tanaka, R. Kato, M. Sasaki and Y. Kagawa: Aip Adv. **4** [2](2014) [in English].
27) T.Z. Zhan, Y.B. Xu, M. Goto, Y. Tanaka, R. Kato, M. Sasaki and Y. Kagawa: Appl Phys Lett. **104** [7](2014) [in English].
28) T. Zhan, Y. Xu, M. Goto, Y. Tanaka, R. Kato and M. Sasaki: Rsc Adv. **5** [61](2015)49703. [in English].
29) M. Goto, M. Sasaki, Y.B. Xu, T.Z. Zhan, Y. Isoda and Y. Shinohara: Appl Surf Sci. **407** (2017)405. [in English].
30) T.Z. Zhan, M. Goto, Y.B. Xu, Y. Kinoshita, M.

Ishikiriyama and C. Nishimura: Rsc Adv. **7** [13](2017)7901. [in English].
31) M. Goto, Y.B. Xu, T.Z. Zhan, M. Sasaki, C. Nishimura, Y. Kinoshita and M. Ishikiriyama: Applied Physics Express. **11** [4](2018) [in English].
32) K. Uchida, M. Sasaki, Y. Sakuraba, R. Iguchi, S. Daimon, E. Saitoh and M. Goto: Scientific Reports. **8** (2018) [in English].
33) Y.J. Wu, M. Sasaki, M. Goto, L. Fang and Y.B. Xu: Acs Appl Nano Mater. **1** [7](2018)3355. [in English].
34) M. Sasaki, S.H. Ju, Y.B. Xu, J. Shiomi and M. Goto: Acs Comb Sci. **22** [12](2020)782. [in English].
35) Y.X. Liao, S. Iwamoto, M. Sasaki, M. Goto and J. Shiomi: Nano Energy. **84** (2021) [in English].
36) M. Sasaki and M. Goto: Thin Solid Films. **761** (2022) [in English].
37) M. Sasaki and M. Goto: J Vac Sci Technol B. **40** [5](2022) [in English].
38) Y.J. Wu, K. Akagi, M. Goto and Y.B. Xu: Int J Heat Mass Tran. **221** (2024) [in English].
39) R. Kato, Y.B. Xu and M. Goto: Jpn J Appl Phys. **50** [10](2011) [in English].
40) T.Z. Zhan, H.D. Wang and Y.B. Xu: Jpn J Appl Phys. **56** [5](2017) [in English].
41) M. Sasaki, Mori, T., Goto, M.: 46th International Symposium on Dry Process, 2025, p. 71.
42) S. Heinz, E.C. Angel, M. Trapp, H.J. Kleebe and G. Jakob: Nanomaterials-Basel. **10** [6](2020) [in English].
43) B.H. Liu, J. Zhou, X.F. Xu and B.W. Li: Nanotechnology. **31** [32](2020) [in English].
44) Y. Zhao, Y. Li, J.X. Qiao, S. Jiang, P.Y. Mao, J.H. Qiu, S.Q. Kang, J. Tan, K.P. Tai and C. Liu: Carbon. **170** (2020)191. [in English].
45) Y.C. Zhao, Z.J. Li, Y.Q. Su, C.Z. Wu and Y. Xie: Acs Nano. (2022) [in English].
46) Y.N. Bai, X. Wang, X.D. Jiang, T.Y. Ouyang, W.Y. Wang, X.R. Li, Y.W. Yan, W. Gao, J.M. Cai, X.M. Cai and H.L. Tan: Mater Today Chem. **42** (2024) [in English].
47) H.W. Hu, Y.Y. Liao, S.S. Tan, C. Li, J. Tang, K. Zheng and L. Yang: Nanoscale. **16** [45](2024)21031. [in English].
48) K.Y. Luo, H.W. Chen, W.Y. Hu, P.P. Qian, J.B. Guo, Y.X. Deng, L. Yang, Q. Sun, L. Liu, L. Cao, W.B. Qiu and J. Tang: Nano Energy. **128** (2024) [in English].
49) D.Y. Wang, J.M. Ding, Y.Q. Mal, C.L. Xu, Z.Y. Li, X. Zhang, Y. Zhao, Y. Zhao, Y.Q. Di, L.Y. Liu, X.J. Dai, Y. Zou, B. Kim, F.J. Zhang, Z.T. Liu, I. McCulloch, M. Lee, C. Chang, X. Yang, D. Wang, D.Q. Zhang, L.D. Zhao, C.A. Di and D.B. Zhu: Nature. **632** [8025](2024)528. [in English].
50) Y.E. Luo, J.L. Zhu, X.R. Rao, Y. Xie, W.X. Ou, R.H. Li and R. Ang: Acs Appl Mater Inter. **17** [5](2025)8047. [in English].
51) S. Radha, J. Mani, A.B.S.S. Andrew, R. Rajkumar, M. Arivanandhan and G. Anbalagan: Mat Sci Semicon Proc. **186** (2025) [in English].
52) Y. Yao, H. Chen, Z.K. Ding, W.H. Xiao, N.N. Luo, J. Zeng, L.M. Tang and K.Q. Chen: J Phys-Condens Mat. **37** [6](2025) [in English].